Doping effects on the electronic and structural properties of CoO$_2$: An LSDA+U study

Peihong Zhang,[1,2] Weidong Luo,[1,2] Vincent H. Crespi,[3] Marvin L. Cohen,[1,2] and Steven G. Louie[1,2]

[1]*Department of Physics, University of California at Berkeley, Berkeley, California 94720, USA*
[2]*Materials Sciences Division, Lawrence Berkeley National Laboratory, Berkeley, California 94720, USA*
[3]*Department of Physics and Materials Research Institute, The Pennsylvania State University, University Park, Pennsylvania 16802, USA*

A systematic local spin density approximation (LSDA)+U study of doping effects on the electronic and structural properties of single layer CoO$_2$ is presented. Undoped CoO$_2$ is a charge transfer insulator within LSDA+U and a metal with a high density of states (DOS) at the Fermi level within LSDA. (CoO$_2$)$^{1.0-}$, on the other hand, is a band insulator with a gap of 2.2 eV. Systems with fractional doping are metals if no charge orderings are present. Due to the strong interaction between the doped electron and other correlated Co d electrons, the calculated electronic structure of (CoO$_2$)$^{x-}$ depends sensitively on the doping level x. Zone center optical phonon energies are calculated under the frozen phonon approximation and are in good agreement with measured values. Softening of the E_g phonon at doping $x \sim 0.25$ seems to indicate a strong electron-phonon coupling in this system. Possible intermediate spin states of Co ions, Na ordering, as well as magnetic and charge orderings in this system are also discussed.

I. INTRODUCTION

The recent discovery of superconductivity in hydrated Na$_x$CoO$_2$ (Ref. 1) has generated renewed interest in this technologically important material. Na$_x$CoO$_2$ has been known for several years as a potential thermoelectric material which exhibits an unexpectedly large thermoelectric power and at the same time a low resistivity.[2] Although the origin of the large thermopower remains a subject of active investigation, strong correlations between Co d electrons and spin entropy are believed to play a critical role.[3–5] In addition to its unusual thermoelectric properties, Na$_x$CoO$_2$ (x in the range 0.5–0.75) is also known for having a Curie-Weiss type of susceptibility instead of a Pauli paramagnetic behavior,[6–8] which would be more compatible with its metallic conduction.[6] Although there have been reports of a weak magnetic ordering transition in Na$_{0.75}$CoO$_2$ at $T_m=22$ K,[8,9] no such transition has been observed down to 2 K for systems with lower Na contents. Compared to the vast experimental work that has been done on this material, theoretical study seems to have lagged behind.

First principle calculations of electronic and magnetic properties of strongly correlated systems such as Na$_x$CoO$_2$ have always been a challenge. Although the local spin density approximation (LSDA) to the density functional theory (DFT) has been applied to various systems with great success, it is well known that the LSDA fails in many aspects when applied to late transition metal oxides in which strong correlations between d electrons play an important role. For example, LSDA fails to reproduce the insulating, antiferromagnetic (AFM) ground state for several transition metal oxides, including the parent materials of high transition temperature (T_c) superconductors. Not surprisingly, there have been several attempts to improve the L(S)DA to take into account (at least partially) the strong electron-electron interactions in first-principle calculations. One of the simplest, yet very successful schemes, was proposed by Anisimov *et al.*:[10–13] the LDA+U method. In this paper, we present a systematic LSDA+U study of doping effects on the electronic and structural properties of Na$_x$CoO$_2$ ($0 \leqslant x \leqslant 1$) using a recently implemented rotationally invariant LSDA+U method [13] within the pseudopotential plane-wave formalism.[14]

II. THE LSDA+U METHOD

It is now well established that the failure of LSDA, when applied to late transition metal oxides, is largely due to an insufficient treatment of on-site Coulomb interactions between the rather localized d electrons. LSDA attempts to account for the Coulomb interaction via an averaged potential depending only on local spin densities. Consequently, magnetic moment formation is driven mainly by the spin polarization energy within LSDA. Orbital polarizations, on the other hand, play less important roles in LSDA and the occupation of localized orbitals does not depend sensitively on their orientation (symmetry). For highly localized electrons, however, the Coulomb interaction should be applied to the localized orbital as a whole and is better described by the Hubbard or Hartree-Fock (HF) type of theory. The formation of a local moment is therefore a result of both spin and orbital polarizations. Unfortunately, although the HF approximation and other correlated quantum chemistry methods have been applied to atomic and molecular systems with tremendous success, their application to solids has been limited. Screening effects, which are relatively weak in atoms and molecules, are usually important in solids and cannot be easily included within the HF theory. Higher level quantum chemistry calculations, on the other hand, are computationally too expensive for most solids.

The LSDA+U method attempts to incorporate the orbital specific screened Coulomb interaction while retaining the simplicity of LSDA. In LSDA+U, the energy functional consists of three contributions [10,11]

$$E^{\text{LSDA}+\text{U}}[\rho^\sigma(\mathbf{r}),\{\mathbf{n}^\sigma\}] = E^{\text{LSDA}}[\rho^\sigma(\mathbf{r})] + E^U[\{\mathbf{n}^\sigma\}] - E^{\text{DC}}[\{\mathbf{n}^\sigma\}], \tag{1}$$

where E^{LSDA} is the usual LSDA energy functional for spin densities ρ^σ ($\sigma = \uparrow, \downarrow$), E^U is a Hubbard or HF type of interaction arising from localized electrons (described by orbital occupation density matrices $\mathbf{n}^\sigma$), and E^{DC} is a "double-counting" term to be defined later. In the rotationally invariant LSDA+U method,[13] E^U takes the familiar HF form

$$E^U = \frac{1}{2} \sum_{\{m\},\{\sigma\}} (\langle m_1, m_2 | V^{ee} | m_3, m_4 \rangle$$

$$- \delta_{\sigma,\sigma'} \langle m_1, m_2 | V^{ee} | m_4, m_3 \rangle) n^\sigma_{m_1,m_3} n^{\sigma'}_{m_2,m_4}, \tag{2}$$

where the matrix elements of the screened electron-electron interaction V^{ee} can be expressed approximately as a sum of Slater integrals F^k:

$$\langle m_1, m_2 | V^{ee} | m_3, m_4 \rangle \approx \sum_{k=0,2}^{2l} a_k(m_1, m_3, m_2, m_4) F^k, \tag{3}$$

$$F^k \approx \frac{1}{\epsilon} \int \frac{r_<^k}{r_>^{k+1}} R_l^2(r_1) R_l^2(r_2) dr_1 dr_2, \tag{4}$$

$$a_k(m_1, m_3, m_2, m_4) = \frac{4\pi}{2k+1} \sum_{q=-k}^{k} \langle Y_{lm_1} | Y_{kq} | Y_{lm_3} \rangle. \tag{5}$$

Here ϵ is the dielectric constant of the system, $r_<$ and $r_>$ are the smallest and largest values of r_1 and r_2, and R_l is the radial wave function of the localized electron. It should be pointed out that the Slater integrals are not well defined in solids and expression (3) is only an approximation. For d electrons ($l=2$), three Slater integrals F^0, F^2, and F^4 are needed. The Slater integrals relate to the familiar Coulomb (or Hubbard) U and exchange J parameters as $U = F^0$ and $J = (F^2 + F^4)/14$. A further simplification can be achieved by the observation that $F^4/F^2 \approx 0.625$ for most d-electron systems.[11,15] The Slater integrals F^k's (or equivalently, U and J) are fixed parameters in our calculations. In principle, however, one could calculate these parameters self-consistently. The double counting term

$$E^{\text{DC}}[\{n^\sigma\}] = U \frac{n(n-1)}{2} - J \left[\frac{n^\uparrow(n^\uparrow - 1)}{2} + \frac{n^\downarrow(n^\downarrow - 1)}{2} \right] \tag{6}$$

is the averaged electron-electron interaction already included in LSDA, assuming that LSDA gives the overall Coulomb and exchange energies correctly. The double counting term is not uniquely defined and there have been some discussions in the literature concerning other possible forms and their effects on the calculated properties.[16] In the above expressions, $n^\sigma = \text{Tr}(\mathbf{n}^\sigma)$ and $n = n^\uparrow + n^\downarrow$, while the density matrix $\mathbf{n}^\sigma$ for localized (e.g., d or f) orbitals remains to be defined. Identifying localized orbitals is trivial in computational methods using atomic basis sets such as the linear muffin-tin orbital method (LMTO). In the pseudopotential plane-wave method, this is less obvious and can be done by projecting the wave functions Ψ^σ_{nk} onto pseudoatomic orbitals $R_l(r)$ cal-

culated with an appropriate atomic configuration ($3d^6 4s^0$ for Co in this work):

$$n^\sigma_{m_1,m_2} = \sum_{n,k} f^\sigma_{nk} \langle m_1 | \Psi^\sigma_{nk} \rangle \langle \Psi^\sigma_{nk} | m_2 \rangle, \tag{7}$$

where f^σ_{nk} is the Fermi occupation factor. We have used the abbreviation $|m\rangle \equiv |R_l Y_{lm}\rangle$. The projection of band wavefunctions Ψ^σ_{nk} onto the pseudoatomic wave function is done in two steps: First, we use the Bessel-Fourier transformation of the band wave function to obtain a radial function $u^\sigma(r)$ centered at the atomic site of interest

$$u^\sigma_{nk,lm}(r) = \langle Y_{lm} | \Psi^\sigma_{nk} \rangle. \tag{8}$$

Next, a numerical integration on a radial grid is carried out to evaluate the overlap $C^\sigma_{nk,lm}$ between the projected radial wave function and the pseudoatomic radial wave function

$$C^\sigma_{nk,lm} = \int_0^{r_c} u^\sigma_{nk,lm}(r) R_l(r) r^2 dr, \tag{9}$$

where r_c is the appropriate cutoff radius (1.2 Å for the Co d orbital in our calculation). Finally the density matrix is constructed:

$$n^\sigma_{m_1,m_2} = \sum_{n,k} f^\sigma_{nk} (C^\sigma_{nk,lm_1})^* C^\sigma_{nk,lm_2}. \tag{10}$$

The LSDA+U wave functions are used to construct the density matrix except at the first step of the self-consistent iteration. Note that proper symmetrizations of the density matrix are needed if the above summation is carried out in the irreducible Brillouin zone (BZ). Diagonalization of the density matrix then gives the symmetry-adapted local orbitals and their occupation numbers.

Applying the variational principle to the energy functionals defined in Eqs. (1), (2), and (6), we have, in addition to the usual one-electron LSDA Hamiltonian, an orbital-dependent correction term

$$\delta \mathbf{V}^\sigma = \sum_{m_1,m_2} |m_1\rangle \delta V^\sigma_{m_1,m_2} \langle m_2|, \tag{11}$$

where the matrix elements

$$\delta V^\sigma_{m_1,m_2} = \sum_{m_3,m_4,\sigma'} (\langle m_1, m_3 | V^{ee} | m_2, m_4 \rangle$$

$$- \delta_{\sigma\sigma'} \langle m_1, m_3 | V^{ee} | m_4, m_2 \rangle) n^{\sigma'}_{m_3,m_4}$$

$$- \delta_{m_1,m_2} \left[U\left(n - \frac{1}{2}\right) - J\left(n^\sigma - \frac{1}{2}\right) \right]. \tag{12}$$

The resulting one-electron problem

$$(H^\sigma_{\text{LSDA}} + \delta \mathbf{V}^\sigma) | \Psi^\sigma_{nk} \rangle = E^\sigma_{nk} | \Psi^\sigma_{nk} \rangle \tag{13}$$

can be solved self-consistently. Due to the presence of the orbital-dependent potential $\mathbf{V}^\sigma$, it is more convenient to solve Eq. (13) in two steps.[17] First, we solve an auxiliary LSDA problem
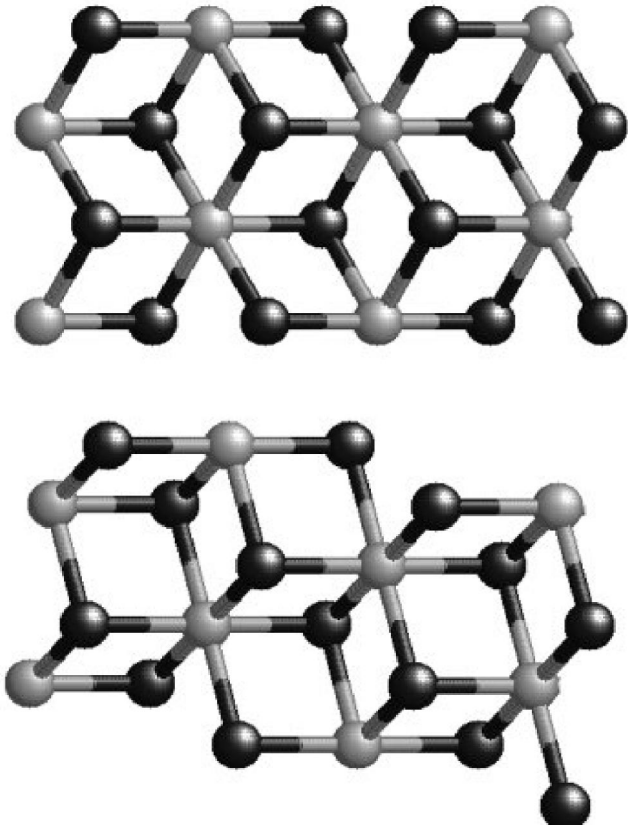
FIG. 1. Orthographic (upper) and perspective (lower) views of single layer CoO_2. Dark spheres are oxygen and gray ones are Co.

$$H^\sigma_{\text{LSDA}}|\Phi^\sigma_{nk}\rangle = \varepsilon^\sigma_{nk}|\Phi^\sigma_{nk}\rangle \qquad (14)$$

to obtain an orthogonal basis $\{\Phi^\sigma_{nk}\}$ and the corresponding eigenvalues $\{\varepsilon^\sigma_{nk}\}$. Note that the one-electron Hamiltonian H^σ_{LSDA} is constructed using the electron density determined by minimizing the LSDA+U (not the LSDA) energy functional. We then construct the full LSDA+U Hamiltonian matrix

$$[H^\sigma_{\text{LSDA+U}}(\vec{k})]_{n,n'} = \delta_{n,n'}\varepsilon^\sigma_{nk} + \langle\Phi^\sigma_{nk}|\delta\mathbf{V}^\sigma|\Phi^\sigma_{n'k}\rangle \qquad (15)$$

on the subspace of interest (e.g., Co d orbitals) and diagonalize it to obtain the LSDA+U wave functions Ψ^σ_{nk} and band energies E^σ_{nk}. The occupation matrix $\mathbf{n}^\sigma$ and charge density ρ^σ are then constructed for the next iteration until the self-consistency is achieved, while fixing the parameters U and J.

III. COMPUTATIONAL DETAILS

Na_xCoO_2 assumes a layered structure in which CoO_2 and Na layers alternate along the c axis. The electronically active CoO_2 layer consists of edge sharing CoO_6 octahedra with magnetic (Co) ions forming a frustrated triangular lattice (see Fig. 1). The oxygen octahedra are distorted considerably—compressed along the body-diagonal direction of the embedding rocksalt structure and stretched in the perpendicular plane. The distortion presumably depends on the doping level (as will be shown later). This active CoO_2 layer is

believed to be responsible for various abnormal electronic, magnetic and transport properties of the system and is the focus of the present study. The sodium layer is disordered, with Na ions distributed among two distinct, partially occupied sites (Wyckoff indices 2b and 2d). In order to avoid inconvenient (i.e., large) unit cells for systems with fractional doping, the effects of Na is modeled by corresponding electron doping into the CoO_2 layer in our calculations. The excess electrons are then balanced by a uniform positive background. In real systems, the presence of Na potentials and small strains associated with them, as well as interlayer interactions, might have some additional effects on the electronic properties. We believe, however, our model captures the essential physics and the effects of Na ions are minor if not negligible, as will be discussed later. (Alternatively, one may employ the virtual crystal technique to overcome the large unit cell problem.) Our treatment might become even more exact in the case of hydrated compounds since water molecules are likely to screen out the Na potentials. Of course, the interaction between H_2O and CoO_2 layers is another issue that deserves further investigations. In our calculations for single layer CoO_2, we fix the in-plane lattice constants $a=b=2.823$ Å,[1] regardless of the doping level. Small variation in lattice constants should have negligible effects on our results. The separation between layers is set at 6.5 Å to ensure no significant interlayer interactions. Therefore, the only structural parameter allowed to relax is the oxygen z coordinate, which turns out to be rather sensitive to the doping level, as will be discussed later.

The above assumptions significantly simplify our calculations. There are, however, other difficulties in studying correlated systems due to the existence of several competing charge and/or magnetic orderings. Since the magnetic and/or charge ordering energies are usually very small, it is sometimes difficult to distinguish between different ordering states based only on their energy difference. This is particularly true in magnetically frustrated systems such as CoO_2, as is evidenced by experiments where no long range magnetic ordering is observed for Na_xCoO_2 except for $x \sim 0.75$.[8,9] Nevertheless, it was suggested that a short range ferromagnetic (FM) ordering might be preferred in these systems.[18] Therefore, we will primary concentrate on the ferromagnetic (paramagnetic for $x=1$) phase in this paper. Different orderings will be discussed briefly.

We employ the LSDA+U method as described in Sec. II to study doping effects on the electronic, structural and magnetic properties of single layer $(CoO_2)^{x-}$ $(0 \leqslant x \leqslant 1)$. The k-point set is generated by the Monkhorst-Pack scheme[19] with a density of $12 \times 12 \times 2$. The plane-wave energy cutoff is set at 250 Ry to ensure the convergence of the calculations. Such a high plane-wave energy cutoff is necessary for systems containing very localized d electrons using norm-conserving pseudopotentials.[20,21] Since there has been no theoretical and/or experimental determination of U and J for Co d electrons in Na_xCoO_2, we adopt a moderate $U=5.5$ eV and a $J=0.9$ eV in our calculations and neglect their doping dependence. The exchange parameter J is of the order of 1 eV for most later transition metal oxides[10] and Singh has given an estimate of $U=5-8$ eV for Na_xCoO_2.[18] Similar values of U (5.4 and 5.0 eV) have been used in previous

studies on this system.[22,23] In general, LSDA+U results are insensitive to small variation of these parameters.

IV. RESULTS

A. Electronic structure of CoO_2 and $CoO_2^{1.0-}$

We first study the undoped parent material CoO_2 in its ferromagnetic phase. Single layer CoO_2 has a D_{3d} point group symmetry, which derives from the cubic (O_h) symmetry after a trigonal distortion along the [111] direction. The Co 3d orbitals split into a triplet (t_{2g}) and a doublet (e_g) under the influence of the octahedral (cubic) crystal field. Upon further lowering the symmetry, the t_{2g} states split into e_g and a_{1g} levels. The t_{2g} derived e_g states then mix with the original e_g ones, forming two new doublets $e_g^{(1)}$ and $e_g^{(2)}$. Of course, the degree of this mixing increases with increasing trigonal distortion and Co d derived e_g states will further hybridize with the O p states. It is generally believed that the relevant low-energy electronic states of CoO_2 are predominately of Co d character and can be interpreted in terms of those of the Co ion. For example, the electronic structure of undoped CoO_2 in its low spin state ($S = \frac{1}{2}$) may be understood in terms of $Co^{4+}(e_g^{\uparrow} a_{1g}^{\uparrow} e_g^{\downarrow})$. Thus upon electron doping, it becomes a doped spin-$\frac{1}{2}$ system. However, due to the strong mixing between O p and Co d states in these systems, the validity of such a simplified picture needs to be carefully examined.

Figure 2 compares the LSDA and LSDA+U density of states (DOS) of CoO_2. The undoped parent material CoO_2 is a Mott-Hubbard insulator (or charge transfer insulator according to the ZAS classification [24]) as predicted by LSDA+U. In contrast, our LSDA calculation gives a metallic ground state with a rather high DOS (2.5 electrons/eV/cell) at the Fermi level, which is consistent with the LSDA result of Singh.[18] The local spin moment of Co calculated within LSDA+U is about $1\mu_B$, as expected for a spin-$\frac{1}{2}$ system. LSDA, on the other hand, gives a local moment of $0.58\mu_B$ due to lack of orbital polarizations. The octahedral crystal field splitting ($\sim$3.0 eV) of Co d orbitals, i.e., the splitting between the occupied t_{2g} and the unoccupied e_g states of the d orbitals, can easily be estimated from the LSDA results. Further splitting of the t_{2g} states [the separation between the two peaks within the triplet labeled $t_{2g}(d+\delta p)$ in the upper panel of Fig. 2] due to the trigonal distortion is about 1.0 eV within LSDA. Determining these values from LSDA+U results, however, is more involved since additional splitting due to the Coulomb U cannot be easily decoupled. The explicit removal of the self-interaction in the screened HF interaction term in the LSDA+U method separates the occupied and the unoccupied d states and pushes the occupied ones below the O p levels. Consequently, the top of the valence band has predominately O p character within LSDA+U, contrary to the Co d character in LSDA. Another interesting observation is that the hybridization between the occupied Co d and O p states is enhanced within the LSDA+U method. Whereas the DOS calculated with LSDA clearly shows p-dominate t_{2g} and e_g states [labeled $t_{2g}(p+\delta d)$ and $e_g(p+\delta d)$ in Fig. 2] and d-dominate t_{2g} states [labeled $t_{2g}(d$
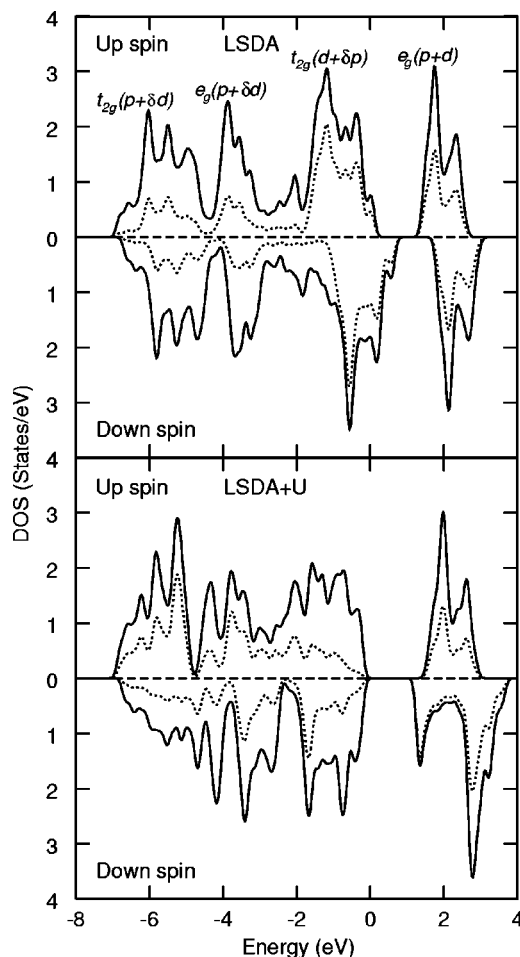

FIG. 2. Spin resolved DOS of CoO_2 in its ferromagnetic phase calculated with LSDA (upper) and LSDA+U (lower). Solid curves show the total DOS and the dotted ones are partial DOS projected on Co d orbitals.

$+\delta p)$], this separation between d and p states becomes less obvious in LSDA+U results. Therefore, our results suggest that both Co d and O p states need to be considered when one attempts to derive an effective low energy model Hamiltonian for this system.

To better understand the electronic structure of CoO_2, we further project the wave functions onto the symmetry-adapted Co d orbitals [i.e., the eigenfunctions of the density matrix defined in Eq. (7)], as shown in Fig. 3. The corresponding orbital occupations are given in Table I. As we have mentioned above, the t_{2g} triplet splits into e_g and a_{1g} under the influence of triangular crystal field. Although this splitting ($\sim$1.0 eV) is insignificant in LSDA, the strong onsite Coulomb interaction included in the LSDA+U pushes the minority spin a_{1g} up so that it becomes completely unoccupied. The separation between the occupied and the unoccupied a_{1g} states is $U+J \sim 6.4$ eV, as shown in the upper panel of Fig. 3. The t_{2g} derived e_g doublet, labeled $e_g^{(2)}$, is nearly fully occupied as expected (see Table I). For the other doublet, i.e., $e_g^{(1)}$, one would expect it to be unoccupied from the simple molecular orbital analysis. However, this does not seem to be the case in our calculations due to strong mixing
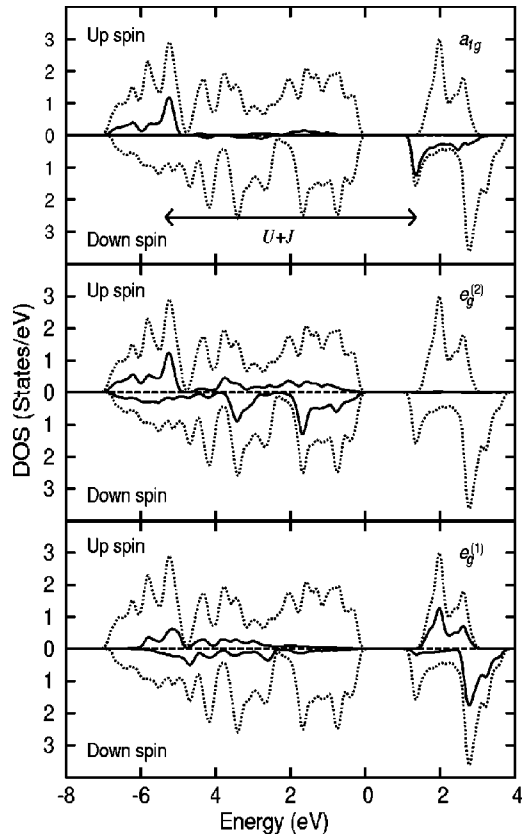
FIG. 3. Local DOS of CoO_2 projected onto the symmetry-adapted Co d orbitals. The total DOS are also shown in dotted curves.
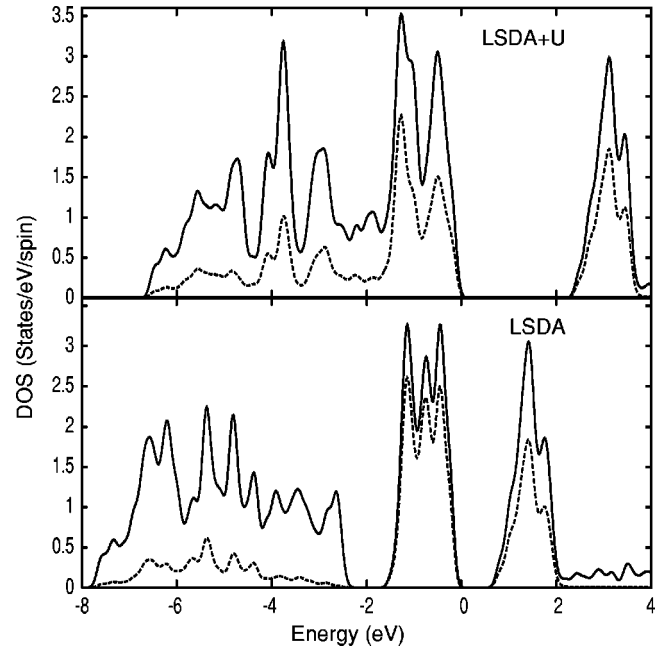

FIG. 4. Comparison between LSDA and LSDA+U DOS of $(CoO_2)^{1.0-}$. Solid curves are total DOS and dotted ones are projections onto Co d orbitals.

between Co d and O p states with compatible symmetry. We call these hybridized doublet $e_g(pd)$. Both the occupied and the unoccupied $e_g(pd)$ have nearly equal O p and Co d characters. As a result, the valency of the Co ion in CoO_2 deviates substantially from its nominal value 4+. This indicates a coexistence of ionic and covalent bondings in this system: Whereas the Co 4s electrons are fully ionized, the d electrons

TABLE I. Comparison of d electron occupation of undoped CoO_2 between LSDA and LSDA+U results. For doublets, the number of d electrons is the occupation times two.

		d orbital	occupation
Majority		LSDA	LSDA+U
spin	a_{1g}	0.845	0.926
	$e_g^{(2)}$	0.907	0.919
	$e_g^{(1)}$	0.457	0.506
Minority	Total	3.57	3.78
spin	a_{1g}	0.668	0.097
	$e_g^{(2)}$	0.725	0.916
	$e_g^{(1)}$	0.434	0.383
	Total	2.99	2.69
Total	d electrons	6.56	6.47
Co spin	moment (μ_B)	0.58	1.09

are better described as covalently bonded with O p electrons due to the significant overlap between the two wave functions.

Upon doping one electron to the CoO_2 layer, the system becomes a nonmagnetic insulator with a band gap of about 2.2 eV (see Fig. 4), which compares favorably with the measured band gap ($\sim$2.7 eV) of a similar material $LiCoO_2$.[25] Interestingly, LSDA also predicts a nonmagnetic insulating ground state but with a smaller gap of about 0.8 eV. This is expected since the crystal field splitting of Co d states within LSDA is larger than the bandwidth of the t_{2g} and e_g subbands. Therefore, $NaCoO_2$ is a band insulator within LDA. The on-site Coulomb interaction thus contributes about 1.4 eV to the calculated band gap, which is only a fraction of the parameter U. This is an indication that the results of LSDA+U calculations are not sensitive to the parameters. Although both LSDA and LSDA+U give qualitatively the same nonmagnetic insulating ground state, there are significant differences in the calculated DOS with the two methods, especially for the occupied states. As for the undoped case, LSDA+U enhances the hybridization between the Co d and O p states. The top valence band triplet has predominately Co d character in the absence of local Coulomb interactions but strongly hybridizes with O p states within LSDA+U. Also, there is a small but not negligible gap between the d-dominate and p-dominate states within LSDA, a feature that does not exist within LSDA+U and was not observed in photoemission experiments.[25] Overall, our results show that the d states mostly concentrate within a 2 eV window below the valence band maximum and the oxygen p states spread from -7.0 to -2.0 eV. This is in good agreement with the resonant photoemission experiment results for $LiCoO_2$ (Ref. 25) where the sharp peak around -1.4 eV is assigned to the Co d final states whereas the broad structure at -5 ± 2 eV is

TABLE II. d electron occupation of $(CoO_2)^{1.0-}$ calculated with LSDA and LSDA+U. The system is nonmagnetic. For doublets, the number of d electrons is the occupation times two.

	d orbital LSDA	occupation/spin LSDA+U
a_{1g}	0.887	0.908
$e_g^{(2)}$	0.889	0.908
$e_g^{(1)}$	0.363	0.321
Total	3.39	3.37

attributed to O p states. Of course, one must be cautious when comparing the calculated DOS with the photoemission results since both matrix element effects and correlations may change the line shape of the photoemission spectra.

The d orbital occupation of both majority and minority spins are significantly affected by the electron doping (see Tables I and II). Whereas the minority spin occupation increases by 0.68 electrons within LSDA+U, the majority spin occupation actually decreases by 0.41. This is not a surprising result for a strongly correlated system: Although the lower and upper Hubbard bands (LHB and UHB) are energetically separated, they are intimately correlated and are both affected by doping. Strong doping dependence of both the band energies and the spectra weights of the correlated d bands can also be seen by comparing the projected DOS between the undoped and doped cases (see the lower panel of Fig. 2 and the upper panel of Fig. 4). Due to their mixing with the correlated d states, O p states are also affected by the doping. Overall, the total d electron occupation only increases by 0.27 electrons upon doping one electron to the system. This suggests that a substantial portion of the doped charge actually go to oxygen sites and that the Co valency is rather insensitive to the doping level in this system. This insensitivity is also recently reported in $Na_xCo_{1-y}Mn_yO_2$ systems, where Co ions are partially substituted by Mn.[26] We will return to this point in more detail later.

To ensure the validity of replacing Na ions with a uniform positive background, which reduces the complex system to a single-layer one, we have also done a calculation for a realistic system, i.e., a double-layer $NaCoO_2$. Figure 5 compares the DOS of the model system $(CoO_2)^{1.0-}$ with that of $NaCoO_2$. The negligible differences between the DOS of the two systems suggest that our model system is appropriate and interlayer coupling is not very important in this system, assuming no charge and/or magnetic orderings are involved. The possibility of a subtle interplay between Na potentials and charge orderings in the CoO_2 layer will be discussed later.

Another issue that needs to be addressed is the effects of variation in the Coulomb U on our results. Although it is known that the LSDA+U results are usually not sensitive to small changes in the U parameter, it is important to understand quantitatively this sensitivity. Table III shows that the change of the d-electron occupation number for both undoped and one electron doped systems is negligible as U is varied from 4.5 to 6.5 eV. Therefore, we believe that our results are quite general and shall be valid for a reasonable range of the U parameter.
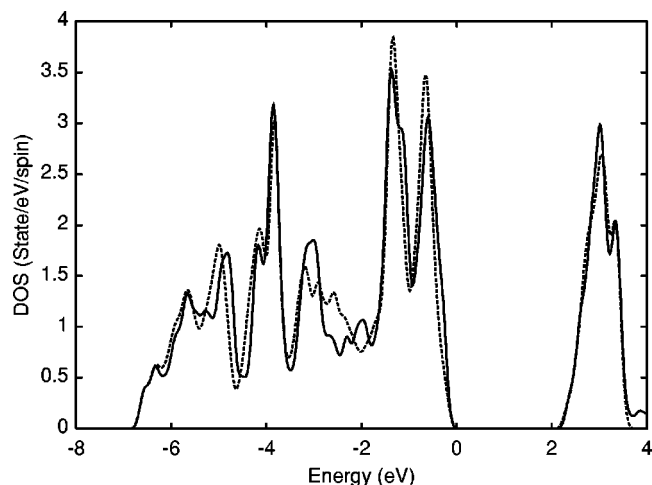

FIG. 5. DOS of $(CoO_2)^{1.0-}$ (solid curve) and that of $NaCoO_2$ (dashed curve). The DOS is not altered significantly by replacing Na ions with a uniform positive background. Also, interlayer coupling does not seem to be important in this system.

B. Electronic structure of $(CoO_2)^{x-}$ ($0 \leq x \leq 1$)

Having discussed the electronic properties of the two extreme cases, it would be interesting to see how the electronic structure of $(CoO_2)^{x-}$ evolves as the doping level x varies. Figure 6 shows the evolution of the DOS as the doping level x changes from 0.0 to 1.0. As we have discussed, the undoped parent material CoO_2 is a charge transfer insulator with a gap between the O p and Co d (a_{1g}) states. Upon electron doping, the originally unoccupied a_{1g} state, which is split-off from the t_{2g} triplet due to on-site Coulomb interactions, becomes partially occupied and moves toward lower energy, touching the O p-dominate valence band at $x \sim 0.3$ and eventually merging into the rest of the valence band. At $x = 1.0$ the t_{2g} triplet is recovered and occupied by both spin up and spin down electrons. At the same time, a new gap (larger than that of the undoped case) appears between the t_{2g} and e_g states. All other occupied d states, in contrast, are pushed upward as doping level increases. As a result, significant spectra weight moves across the entire valence bandwidth due to the correlation between the doped electron and other occupied d states. Note also that the occupation of the minority spin a_{1g} state is approximately the same as the doping level x, which seems to suggest that all doped charges go to Co sites. In fact, this is not true. As we have discussed briefly for the case of $(CoO_2)^{1.0-}$, a significant portion of the doped electron actually goes to oxygen sites. Below we ex-

TABLE III. Sensitivity of the charge occupation analysis to the variation in the U parameter.

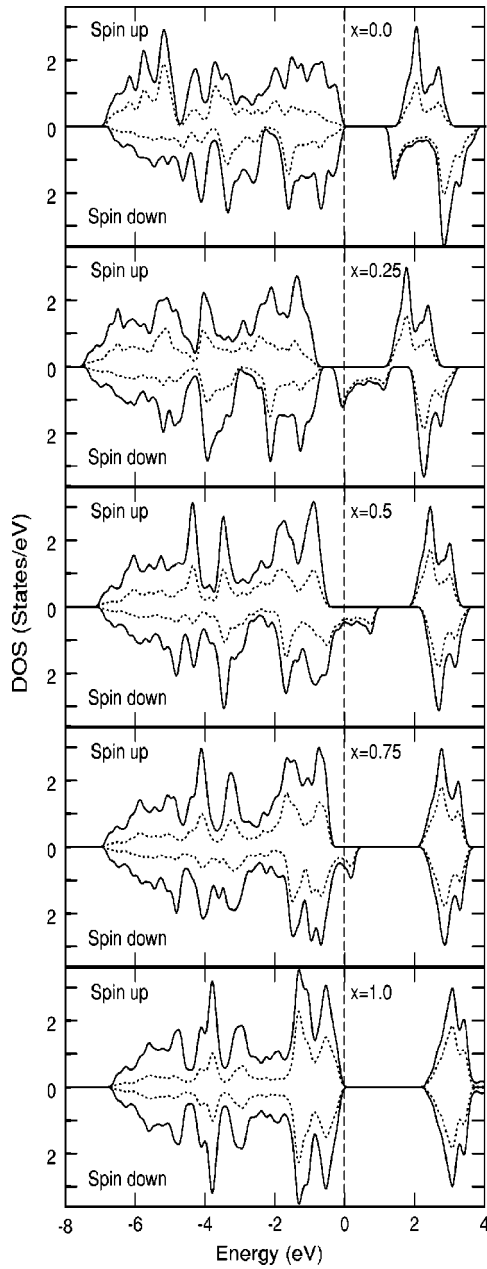|	Number of d electrons	
U	$x=0.0$	$x=1.0$
4.5	6.48	6.75
5.5	6.47	6.73
6.5	6.46	6.72

FIG. 6. Doping effects on the DOS of $(CoO_2)^{x-}$ $(0.0 \leqslant x \leqslant 1.0)$. Solid curves are total DOS and the dotted ones are projections onto Co d orbitals. As the doping level increases, the partially occupied minority spin a_{1g} state moves across the band gap while pushing other correlated d states upwards. The dashed line shows the Fermi level of metallic systems.

amine in more detail these seemingly incompatible results.

Table IV shows the d electron occupations for all symmetrized d orbitals. The occupation of all other d states except the minority spin a_{1g} decreases as doping level increases, with the $e_g^{(1)}$ states (especially the majority spin one) being affected the most (see also Fig. 7). In other words, the occupation of the minority spin a_{1g} state effectively repels other d electrons in the $e_g^{(1)}$ states. This is only possible through the rehybridization process. As mentioned previously, the occupation of the Co-d derived $e_g^{(1)}$ states is due to the hybridiza-

TABLE IV. d electron occupation and local spin moment of $(CoO_2)^{x-}$ as a function of doping level. For doublets, the number of d electrons is the occupation times two.

Doping		0.0	0.25	0.5	0.75	1.0
Majority spin	a_{1g}	0.926	0.922	0.917	0.912	0.908
	$e_g^{(2)}$	0.919	0.916	0.914	0.911	0.908
	$e_g^{(1)}$	0.506	0.436	0.381	0.345	0.321
	total	3.78	3.63	3.51	3.42	3.37
Majority spin	a_{1g}	0.097	0.341	0.566	0.754	0.908
	$e_g^{(2)}$	0.916	0.913	0.910	0.908	0.908
	$e_g^{(1)}$	0.383	0.379	0.367	0.346	0.321
	total	2.69	2.93	3.12	3.26	3.37
Co spin moment (μ_B)		1.08	0.70	0.39	0.16	0.0

tion between p and d orbitals. In the absence of hybridization, the total d electron occupation increases linearly with doping level x ($N_d = N_0 + x$, where N_0 is the d occupation without electron doping). Consequently, the on-site Coulomb interaction energy would increase rapidly since $E^U = U N_d (N_d - 1)/2$. This is obviously very energetically unfavorable. Fortunately, the hybridization process brings in another degree of freedom and the system spontaneously adjusts the level of hybridization to minimize the overall Coulomb energy as doping increases. This competition between the Coulomb energy and the p-d hybridization was also proposed recently by Marianetti *et al.*,[27] although they reach the conclusion based on a dynamical mean-field theory (DMFT) analysis. We should point out that the occupation analysis in our calculations is only approximate and different charge analyses may give slightly different results. The subtle changes to the $e_g^{(2)}$ and majority spin a_{1g} occupation might be partially due to orbital and/or structural relaxation effects.

Another consequence of the rehybridization process is that the effective Coulomb repulsion "felt" by the minority
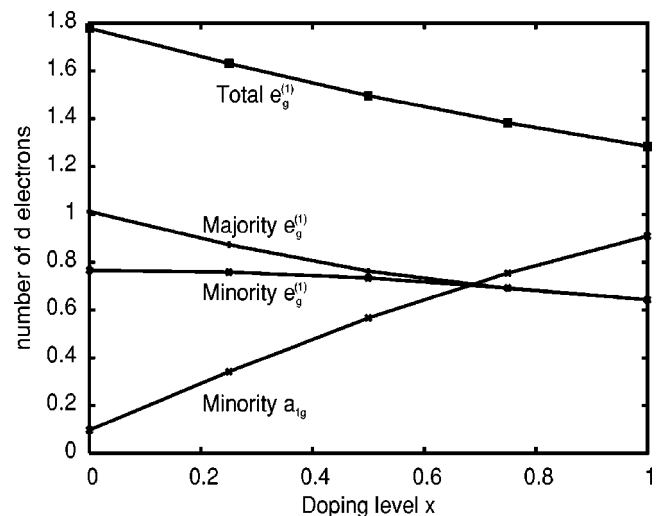

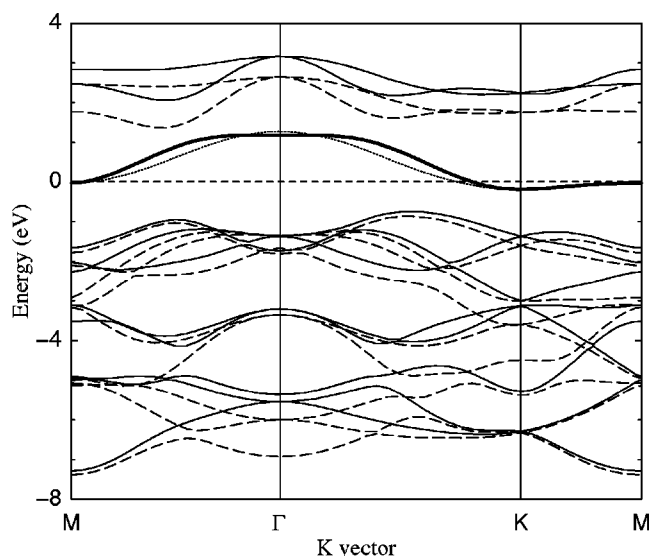FIG. 7. Doping dependence of the occupation of Co d orbital derived a_{1g} and $e_g^{(1)}$ states.

FIG. 8. Band structure of $(CoO_2)^{0.25-}$. Solid and dashed curves are for minority and majority spins, respectively. The minority spin a_{1g} band is highlighted with a thick solid curve and the dotted curve is a nearest neighbor tight-binding fitting for this band with a hopping parameter $t=0.155$ eV.

FIG. 9. Density of states of $(CoO_2)^{1.0-}$ at the Fermi level as a function of doping level x.

spin a_{1g} electron is actually reduced with increasing doping level. This explains the lowering of the energy of the minority spin a_{1g} (relative to other d states) upon electron doping. Of course, other factors might also contribute to the doping dependence of the energy of the minority spin a_{1g} state. For example, the doping-dependent trigonal distortion will change the energy of the a_{1g} state through crystal field splitting effects.

The minority spin a_{1g} state deserves particular attention since, upon electron doping, it determines the low-energy electronic properties of the system and has been the subject of intensive discussion concerning its connection with the superconductivity observed in $Na_{0.3}CoO_2 \cdot yH_2O$.[28–32] Figure 8 shows the band structure of $(CoO_2)^{0.25-}$ with the minority spin a_{1g} band highlighted. Interestingly, apart from a constant shift, this band can be fairly well fitted by a simple tight-binding model with a nearest hopping parameter $t=-0.155$ eV. Note that here t is not the hopping element between Co and O sites but the effective hopping between neighboring Co sites. The total bandwidth is thus $9|t|=1.4$ eV. Since we use a on-site Coulomb interaction $U=5.5$ eV, the effective superexchange between two neighboring Co ions is $J=4t^2/U=16$ meV, in reasonable agreement with a previous estimate.[31] Due to the particular dispersion and doping dependence of this band, there is a strong doping dependence to the Fermi-surface properties and the DOS at the Fermi level, as shown in Fig. 9. The DOS (E_f) increases sharply with increasing doping level for $x \lesssim 0.1$, reaches a maximum at about $x \sim 0.2$, and then decreases with increasing doping. The narrow doping range $0.1 \lesssim x \lesssim 0.3$ beyond which DOS (E_f) decreases rapidly with increasing or decreasing doping level is closely related to the Fermi surface structure of the system: At very low dopings, small electron pockets appear around the corners of the BZ. (Note that this metallic state may not be stable against charge orderings at
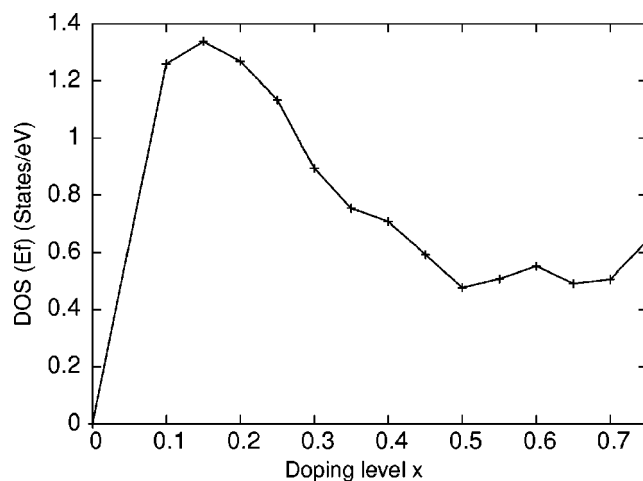
very low doping levels.) The Fermi surface quickly extends and then shrinks with increasing doping. Compared with LSDA results [18] where a large Fermi surface, as well as small pockets of holes, are predicted, there is only one large Fermi surface in our calculation, which agrees well with recent experiments.[33,34] Although it would be interesting to connect this observation with the fact that superconductivity occurs only in a very narrow doping range [$x \sim 0.3$ in $Na_xCoO_2 \cdot yH_2O$ (Refs. 1 and 35)], further investigation on this subject is required. If the superconductivity in this system is of phonon origin, then the high DOS at the Fermi level is definitely an important factor in determining the superconducting transition temperature.

C. Doping effects on the structural properties and possible spin-phonon interactions

Structural properties are in general not particularly sensitive to the doping level. As we have mentioned above, we fix the lattice constants in our calculations but allow the oxygen atoms to relax. Figure 10 shows the doping-dependent oxygen z coordinate as measured from the Co plane. The calculated O z coordinate at $x \sim 0.30$ (1.72 a.u.) falls within the measured values (1.67–1.77 a.u.) for $Na_xCoO_2 \cdot yH_2O$ (Refs. 1 and 36) but is smaller than those (~ 1.83 a.u.) for unhydrated systems.[36] This is reasonable since the single layer system in our calculations should mimic the hydrated system better than the unhydrated one. The Na potential in the unhydrated system is likely to attract the negatively charged O ions away from the Co layer, making the O z coordinate larger. Overall, the distance between the oxygen and cobalt layers expands quadratically with increasing doping level.

Using the LSDA+U total energy functional defined in Eq. (1), we can calculate phonon energies under the frozen phonon approximation.[40] Single layer CoO_2 (assuming paramagnetic/ferromagnetic ordering) has four zone-center optical phonon modes. Two of them relate to the in-plane and out-of-plane motion of oxygen atoms (E_g and A_{1g}), which are Raman active. The other two (E_u and A_{2u}) involve cobalt moving against oxygen and are infrared (IR) active. Table V
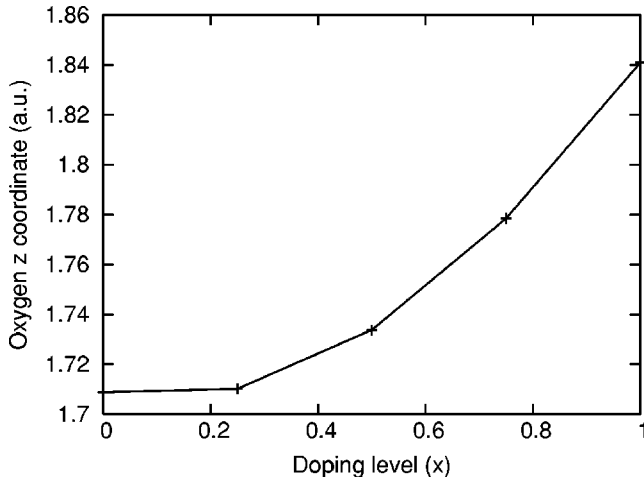
FIG. 10. Calculated equilibrium oxygen z coordinate of $(CoO_2)^{x-}$ as a function of doping level x.

FIG. 11. Correlation between the local spin moment on Co and the oxygen z coordinate of CoO_2.

lists the calculated zone center phonon energies for doping levels $x=0.0, 0.25, 0.5, 0.75$, and 1.0. The calculated energies are in good agreement with available measurements.[37–39] For example, the measured A_{1g} phonon energy [ranging from 71.2 to 74.4 meV (Refs. 37 and 38) depending on the doping level and sample conditions] agrees well with the calculated ones (from 72.6 to 73.0 meV for doping level $0.25 \leqslant x \leqslant 0.75$). The theoretical E_g phonon energies are 63.2 meV for $x=0.25$ and 65.6 meV for $x=0.75$, to be compared with the measured values 56.8–61.2 meV.[37] The measured energy for the IR active mode E_u is about 70.7 meV for $Na_{0.57}CoO_2$,[39] which also compares favorably with our theoretical value (74.7 meV for $x=0.5$). There has been no measurement for the A_{2u} mode so far. In general, the zone center optical phonons are not sensitive to the doping level. There is, however, one interesting exception: At ~ 0.25 doping, the E_g phonon softens, decreasing from 67.8 meV for $x=0.0$ to 63.2 meV for $x=0.25$, and has significant anharmonicity. (The calculated harmonic phonon energy is only 56.5 meV.) The softening of this phonon mode at doping level $x \leqslant 0.2$ seems to indicate a strong electron-phonon coupling and we believe that the high DOS at the Fermi level for $x \sim 0.25$, together with strong electron-phonon couplings between this mode and conduction states, is responsible for the phonon softening and anharmonicity and may eventually lead to a superconducting phase transition.

TABLE V. Doping effects on zone center phonon energies calculated using frozen phonon approximation. All phonon modes are fairly harmonic except the E_g mode in the case of doping level $x \sim 0.25$. For $x=0.25$, the calculated harmonic frequency is shown in parentheses.

	Zone center phonon energy (meV)				
Doping level	0.0	0.25	0.5	0.75	1.0
A_{1g}	72.3	72.6	73.4	73.0	71.4
A_{2u}	72.8	73.6	74.0	77.0	80.0
E_g	67.8	63.2 (56.5)	64.6	65.2	62.7
E_u	75.3	74.9	74.7	74.2	72.7
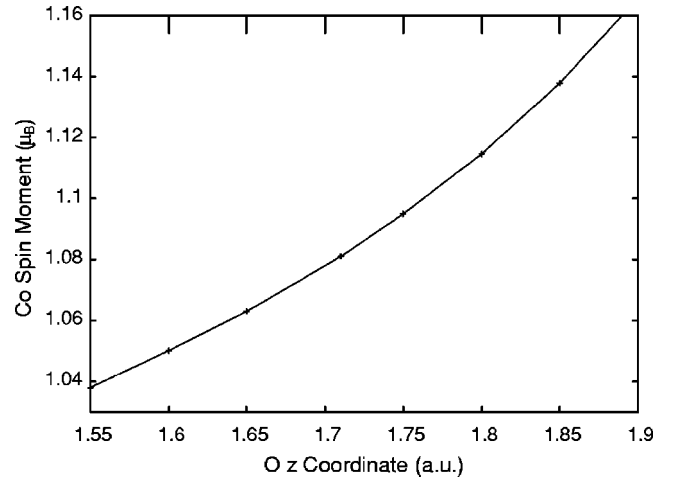
In magnetic systems, phonons might interact with the spin degree of freedom through the magnetoelastic coupling. The spin-phonon interaction has been discussed extensively in the literature regarding its possible role in high-T_C superconductors. Although there is no experimental evidence of a strong spin-phonon coupling in this system so far, it would be interesting to explore such a possibility. In fact, we observe a strong correlation between the O z coordinate (relates to the A_{1g} phonon displacement) and the local spin moment on Co sites (see Fig. 11). No such correlations were found for other phonon modes. This raises the possibility of interactions between A_{1g} phonons and magnons with compatible wave vectors and might have important implications for understanding the superconducting mechanism in this system.

V. DISCUSSIONS

A. Other possible spin configurations

So far we have assumed a low spin state for Co ions and the doped electrons always go to the minority spin a_{1g} conduction band. Thus the local spin moment on Co decreases with increasing doping level and vanishes at $x=1.0$. However, this does not seem to be consistent with the observations that sizable effective magnetic moments μ_{eff} exist at doping level $x \sim 0.75$. For example, magnetic susceptibility measurements of $Na_{0.75}CoO_2$ give a μ_{eff} of $2.74\mu_B$/Co assuming only Co^{4+} ions contribute to the Curie constant C.[8] This is much larger than the "spin-only" value $[g\sqrt{s(s+1)} = \sqrt{3}\mu_B]$ of Co^{4+} ion in its low spin state. If, on the other hand, all Co sites are assumed equivalent, the results yield a μ_{eff} of $1.37\mu_B$/Co,[8] which is again not compatible with the calculated spin moment. This apparent discrepancy raises the possibilities of unquenched orbital moments and/or other spin configurations of Co ions in this system, especially for high doping levels ($x \gtrsim 0.5$). The spin states of Co ions in CoO_2 are determined by several competing factors such as the crystal field splitting, Hund's rule coupling, and the screened on-site Coulomb interactions. Therefore, depending on the relative strength of these factors, some Co ions might

adopt an intermediate-spin state. Here we explore such a possibility.

As we can see from Fig. 2, the energy of the unoccupied majority spin e_g is only slightly higher than that of minority spin a_{1g} in the undoped single layer CoO_2. In the real system, especially in unhydrated Na_xCoO_2, however, the situation might be more complicated. The presence of a ordered Na potential might enhance or induce charge orderings in the CoO_2 layer[41] and the energy levels of the two unoccupied states e_g and a_{1g} might get reversed on some Co sites. A smaller crystal field splitting or larger U could pull down the e_g state or push up the a_{1g} one. The doped electron could then go to the e_g majority spin state, resulting in an intermediate-spin state for the corresponding Co ions. Therefore, we propose the following scenario for unhydrated Na_xCoO_2 system: At low doping level, all Co ions are in their low spin states. As doping level increases, Na ions tend to order themselves to minimize the Coulomb energy. (We will discuss Na orderings in more detail in the following.) This ordering might then enhance or induce charge ordering in CoO_2 layers. Due to charge ordering in the CoO_2 layer, Co ions then have a different symmetry and chemical environment, leading to different crystal field splitting and/or on-site interactions. Under certain circumstance, the unoccupied majority spin e_g state might be lower in energy than the a_{1g} state. The local moment of these Co ions will then increase with increasing doping. We have calculated a ferromagnetic system with Co ions in their intermediate spin states for doping level $x=0.5$ and found that the local spin moment is $1.52\mu_B/Co$. Not surprisingly, the energy of the intermediate spin state is higher than that of the low-spin state (by ~ 0.5 eV/Co). However, charge orderings might reduce or inverse this energy difference, resulting in an intermediate-spin ground state. It is also plausible that this kind of rich degeneracy of spin states, a result of nearly perfect balance between the crystal field and Hund's rules effects, is responsible for the unusually high thermopower in this system.

B. Na ordering, magnetic and/or charge orderings

It is usually assumed that the Na layer is disordered in Na_xCoO_2 and the primary effect of Na is to provide electrons to the CoO_2 layer. In strongly correlated systems, however, charge and/or spin orderings usually happen at an extremely low energy scale and seemingly insignificant interactions can sometimes result in profound changes in the electronic structure. Although we have shown that the Na potential has minimal effects on the calculated electronic structure of ferromagnetically ordered CoO_2, it is still unclear the exact role Na plays in determining the properties of the system, especially at high doping when the Na layer is likely ordered. Whether or not Na becomes ordered depends on a competition between entropic and energetic factors. If energetics dominate, an ordering might occur. In fact, there has been increasing experimental evidence that the Na layer might be ordered at some doping levels. Foo *et al.* observed a $\sqrt{3}\times 2$ ordering in $Na_{0.5}CoO_2$ and discussed the possible effects of Na ordering on its electronic properties.[41] Shi *et al.* reported a 2×1 superstructure in Na_xCoO_2 for $x\geq 0.75$ and ascribed it to a possible Na ordering.[42]

Since Na are fully ionized, it might be possible to discuss their ordering by simple electrostatic and entropic arguments. (Chemical interactions between Na and CoO_2 layers might also play a minor role but more difficult to characterize.) At low Na concentrations, entropic effects should dominate and the Na layer is likely disordered. As doping level increases, however, Na ions will tend to organize themselves (at least partially and locally) to minimize the ionic repulsion, since it costs energy to place two Na ions in neighboring $2b$ and $2d$ sites (see Fig. 12). This does not necessarily lead to a long-range ordering since there could be many (nearly) degenerate local orderings. However, if there exist an ordered pattern which has significantly lower energy (compared to the thermal energy) than others, a long range ordering might result. For $x=0.5$, we indeed find a particular arrangement of Na ions which is compatible with the observed $\sqrt{3}\times 2$ ordering [41] and has as much as 0.3 eV/Na lower Coulomb energy than other configurations with similar unit cells (see Fig. 12) if only in-plane Coulomb interactions are taken into account. It might be possible that the interplay between the ordering in the Na layer and the charge ordering in the CoO_2 layer is responsible for the observed insulating behavior in $Na_{0.5}CoO_2$, as discussed by Foo *et al.*[41] For $x=0.75$, the situation is more complicated. We find many possible orderings with similar energy. The lowest-energy pattern is show in Fig. 12, with filled black circles denoting occupied and gray circles partially occupied (50% for $x=0.75$) Na sites. Interestingly, this pattern of low energy ordering is also consistent with the reported Na superstructure for $x\geq 0.75$.[42] The low energy ordering pattern for $x=0.5$ is rather exclusive in the sense that further addition of Na to this structure will result in occupation of neighboring $2b$ and $2d$ sites thus increase the Coulomb energy sharply.

In general, we find it very energetically unfavorable to occupy neighboring $2b$ and $2d$ sites. At high doping (e.g., $x\geq 0.75$), Na ions tend to occupy only one of the two distinct sites within a given domain. The size of these domains presumably increases with decreasing temperature. If interactions between Na and CoO_2 layers are taken into account, the two Na sites may not be equivalent energetically. In fact, our calculations indicate that the $2d$ site is about 0.1 eV/Na lower in energy. This is due to the different Coulomb repulsion between the Na and Co in the two configurations. Therefore, $2d$ sites are more likely to be occupied, provided that no immediate neighboring $2b$ sites are already occupied. Although this differentiation between the two sites should be taken into account when discussing Na orderings, no changes to our conclusion for a Na ordering of $x=0.5$ is expected due to the large in-plane ordering energy.

Magnetic and/or charge orderings in Na_xCoO_2 are other subjects of great interest. Kunes *et al.*,[22] and Motrunich *et al.*,[43] discussed a possible $\sqrt{3}\times\sqrt{3}$ charge ordering for doping $x\sim\frac{1}{3}$. Foo *et al.* reported a $\sqrt{3}\times 2$ Na ordering at $x=0.5$ as we have mentioned above. NMR measurements also point to possible charge orderings in Na_xCoO_2 for $0.5\leq x\leq 0.75$.[44,45] However, there is no consensus in the literature on this matter so far. The magnetic ordering in Na_xCoO_2 is even more intriguing. Very weak magnetic ordering has been observed at $T\sim 22$ K only for doping $x\sim 0.75$. Curiously enough, the measured magnetizations differ by two order of
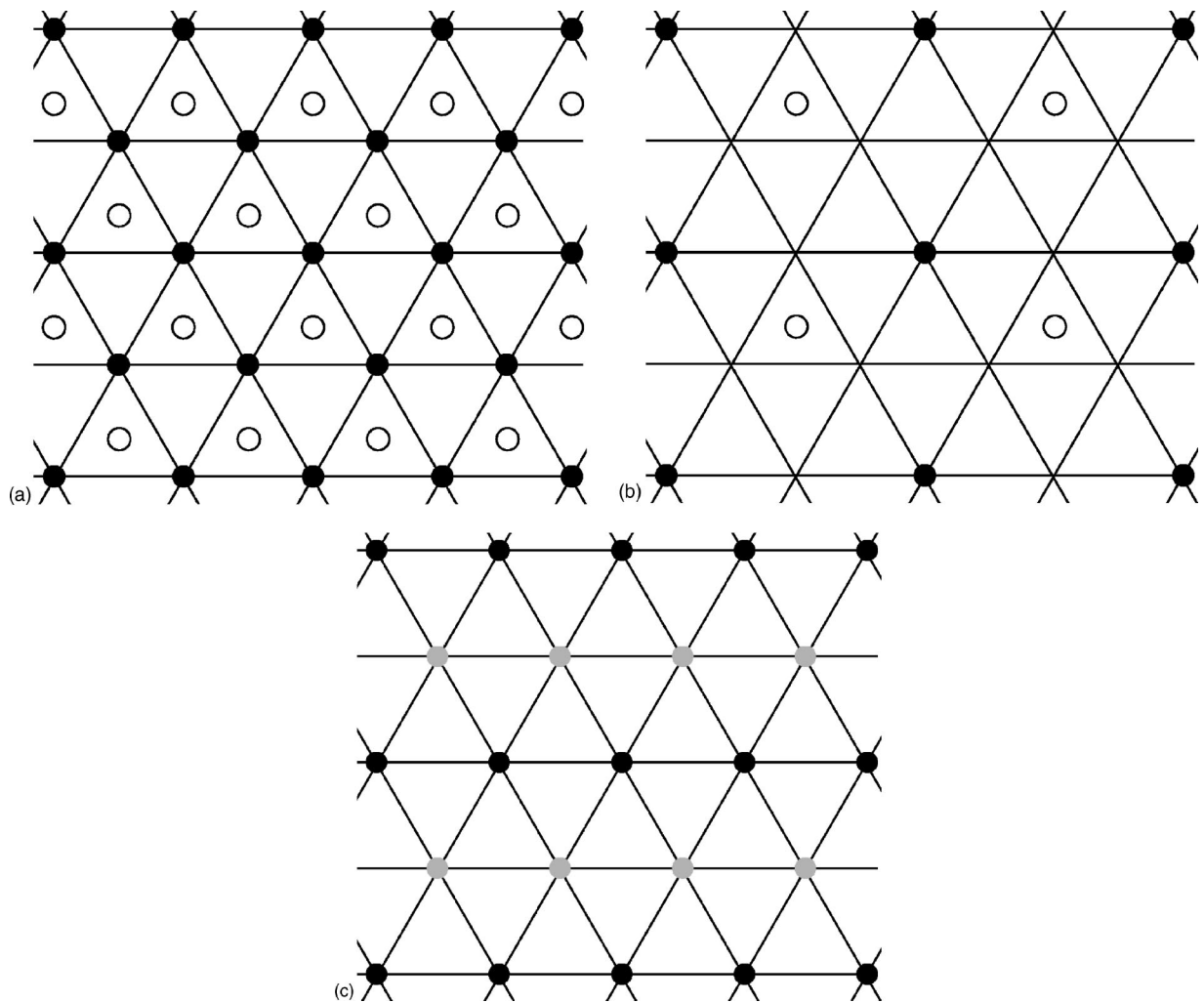
FIG. 12. Possible Na ordering patterns. Upper: Two distinct Na sites in Na_xCoO_2. At doping $x=1.0$, Na will occupy only one of the two sites at low temperature. Middle: Lowest-energy ordering pattern for $x=0.5$. Lower: A low-energy ordering pattern for $x=0.75$. Gray circles indicate partially (50%) occupied Na sites.

magnitude between two experiments.[8,9] We try to explore the simplest AFM ordering with a 2×1 unit cell in this system. The AFM phase is found to be slightly lower in energy (~ 10 meV/Co) than the FM phase for doping level $x=0.3$. However, this small difference could be beyond the accuracy of our theoretical treatment. Figure 13 compares the calculated DOS of FM and AFM phases of $(CoO_2)^{0.3-}$. Although the low energy valence states are not significantly affected, the bandwidth of the partially occupied a_{1g} state is greatly reduced as a result of AFM ordering. This raises the possibility of further suppression of the a_{1g} bandwidth if more complicated orderings are present, which might help to account for the mysterious electron mass enhancement[32] in this system. Unfortunately, due to the extremely small energy differences between competing ordering states, fluctuations among these states result in very slow convergence in self-consistent calculations.

VI. CONCLUSION

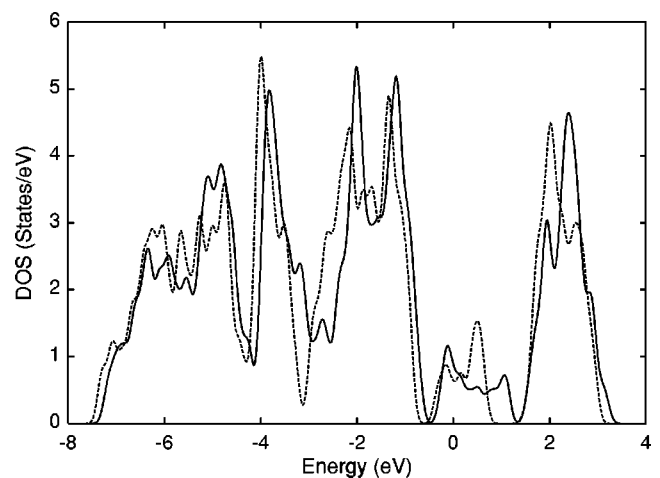In conclusion, we have carried out systematic studies on the electronic, magnetic and structural properties of single

FIG. 13. Magnetic ordering effects on the electronic structure of $(CoO_2)^{0.3-}$. The solid curve is for the FM phase and the dotted curve for the AFM phase. Although no significant changes to low-lying valence states are observed, the width of the a_{1g} conduction band is renormalized (narrowed) appreciably due to the ordering.

layer $(CoO_2)^{x-}$ using a recently implemented rotationally invariant LSDA+U method within the pseudopotential plane-wave formalism. Both the undoped and one integer electron doped systems are insulators within LSDA+U, whereas systems with fraction doping are half metal in the absence of charge ordering and assuming a ferromagnetic phase. Calculated Fermi surface and zone center phonon energies agree well with available measurements. Possible intermediate spin configurations of Co ions, Na orderings, and magnetic and charge orderings in this system are also discussed.

Although the pairing mechanism that leads to supercondictivity in this system remains a subject of intensive investigation, high DOS at the Fermi level at low doping levels, together with strong electron-phonon couplings and possible spin-phonon interactions, might be partially responsible for the superconducting transition in the hydrated systems. The role water molecules play in the superconducting transition is still unknown. One possibility is that the screening effects, which greatly suppress the interaction between Na and CoO_2

layers and possible charge orderings in the CoO_2 layer, lead to a more homogeneous electronic system in the CoO_2 layer and ultimately favor a superconducting state over competing phases. A better understanding of the properties of this material requires more experimental work and thorough theoretical investigations. The interplay between the Na ordering and the charge/magnetic ordering in the CoO_2 layer deserves particular attention, especially in the unhydrated system.

[1] K. Takada, H. Sakural, E. Takayama-Muromachi, F. Izumi, R. A. Dilanian, and T. Sasaki, Nature (London) **422**, 53 (2003).

[2] I. Terasaki, Y. Sasago, and K. Uchinokura, Phys. Rev. B **56**, R12 685 (1997).

[3] Y. Ando, N. Miyamoto, K. Segawa, T. Kawata, and I. Terasaki, Phys. Rev. B **60**, 10 580 (1999).

[4] W. Koshibae, K. Tsutsui, and S. Maekawa, Phys. Rev. B **62**, 6869 (2000).

[5] Y. Wang, N. Rogado, R. J. Cava, and N. P. Ong, Nature (London) **423**, 425 (2003).

[6] T. Tanaka, S. Nakamura, and S. Iida, Jpn. J. Appl. Phys., Part 2 **33**, L581 (1994).

[7] R. Ray, A. Ghoshray, and K. Ghoshray, Phys. Rev. B **59**, 9454 (1999).

[8] T. Motohashi, R. Ueda, E. Naujalis, T. Tojo, I. Terasaki, T. Atake, M. Karppinen, and H. Yamauchi, Phys. Rev. B **67**, 064406 (2003).

[9] J. Sugiyama, H. Itahara, J. H. Brewer, E. J. Ansaldo, T. Motohashi, M. Karppinen, and H. Yamauchi, Phys. Rev. B **67**, 214420 (2003).

[10] V. I. Anisimov, J. Zaanen, and O. K. Andersen, Phys. Rev. B **44**, 943 (1991).

[11] V. I. Anisimov, I. V. Solovyev, M. A. Korotin, M. T. Czyżyk, and G. A. Sawatzky, Phys. Rev. B **48**, 16 929 (1993).

[12] M. T. Czyżyk and G. A. Sawatzky, Phys. Rev. B **49**, 14 211 (1994).

[13] A. I. Liechtenstein, V. I. Anisimov, and J. Zaanen, Phys. Rev. B **52**, R5467 (1995).

[14] J. Ihm, A. Zunger, and M. L. Cohen, J. Phys. C **12**, 4409 (1979).

[15] F. M. F. de Groot, J. C. Fuggle, B. T. Thole, and G. A. Sawatzky, Phys. Rev. B **42**, 5459 (1990).

[16] A. G. Petukhov, I. I. Mazin, L. Chioncel, and A. I. Lichtenstein, Phys. Rev. B **67**, 153106 (2003).

[17] A. B. Shick, A. I. Liechtenstein, and W. E. Pickett, Phys. Rev. B **60**, 10 763 (1999).

[18] D. J. Singh, Phys. Rev. B **61**, 13 397 (2000).

[19] H. J. Monkhorst and J. D. Pack, Phys. Rev. B **13**, 5188 (1976).

[20] D. R. Hamman, M. Schluter, and C. Chiang, Phys. Rev. Lett. **43**, 1494 (1979).

[21] N. Troullier and José Luís Martins, Phys. Rev. B **43**, 1993 (1991).

[22] J. Kunes, K.-W. Lee, and W. E. Pickett, cond-mat/0308388 (unpublished).

[23] L. Zuo, J. Wang, and Z. Zeng, cond-mat/0307560 (unpublished).

[24] J. Zaanen, G. W. Sawatzky, and J. W. Allen, Phys. Rev. Lett. **55**, 418 (1985).

[25] J. van Elp, J. L. Wieland, H. Eskes, P. Kuiper, and G. A. Sawatzky, Phys. Rev. B **44**, 6090 (1991).

[26] W. Y. Zhang, H. C. Yu, Y. G. Zhao, X. P. Zhang, Y. G. Shi, Z. H. Cheng, and J. Q. Li, cond-mat/0312086 (unpublished).

[27] C. C. Marianetti, G. Kotliar, and G. Ceder, cond-mat/0312514 (unpublished).

[28] G. Baskaran, Phys. Rev. Lett. **91**, 097003 (2003).

[29] A. Tanaka and X. Hu, Phys. Rev. Lett. **91**, 257006 (2003).

[30] C. Honerkamp, cond-mat/0304460 (unpublished).

[31] Q. Wang, D. Lee, and P. A. Lee, cond-mat/0304377 (unpublished).

[32] F. C. Chou, J. H. Cho, P. A. Lee, E. T. Abel, K. Matan, and Y. S. Lee, cond-mat/0306659 (unpublished).

[33] M. Z. Hasan, Y. D. Chuang, A. P. Kuprin, Y. Kong, D. Qian, Y. W. Li, B. L. Mesler, Z. Hussain, A. V. Fedorov, R. Kimmerling, E. Rotenberg, K. Koh, M. Rogado, M. L. Foo, and R. J. Cava, cond-mat/0308438 (unpublished).

[34] H.-B. Yang, S.-C. Wang, A. K. P. Sekharan, H. Matsui, S. Souma, T. Sato, T. Takahashi, T. Takeuchi, J. C. Campuzano, R. Jin, B. C. Sales, D. Mandrus, Z. Wang, and H. Ding, cond-mat/0310532 (unpublished).

[35] R. E. Schaak, T. Klimczuk, M. L. Foo, and R. J. Cava, Nature (London) **424**, 527 (2003).

[36] J. W. Lynn, Q. Huang, C. M. Brown, V. L. Miller, M. L. Foo, R. E. Schaak, C. Y. Jones, E. A. Mackey, and R. J. Cava, Phys. Rev. B **68**, 214516 (2003).

[37] M. N. Iliev, A. P. Litvinchuk, R. L. Meng, Y. Y. Sun, J. Cmaidalka, and C. W. Chu, Physica C **402**, 239 (2004).

[38] P. Lemmens, V. Gnezdilov, N. N. Kovaleva, K. Y. Choi, H. Sakurai, E. Takayama-Muromachi, K. Takada, T. Sasaki, F. C. Chou, C. T. Lin, and B. Kermer, cond-mat/0309186 (unpublished).

[39] S. Lupi, M. Ortolani, and P. Calvani, cond-mat/0312512 (unpublished).

[40] See, for example, M. T. Yin and M. L. Cohen, Phys. Rev. B **26**, 3259 (1982).

[41] M. L. Foo, Y. Wang, S. Watauchi, H. W. Zandbergen, T. He, R. J. Cava, and N. P. Ong, cond-mat/0312174 (unpublished).

[42] Y. G. Shi, H. C. Yu, C. J. Nie, and J. Q. Li, cond-mat/0401052 (unpublished).

[43] O. I. Motrunich and P. A. Lee, cond-mat/0310387 (unpublished).

[44] J. L. Gavilano, D. Rau, B. Pedrini, J. Hinderer, H. R. Ott, S. M. Kazakov, and J. Karpinski, cond-mat/0308383 (unpublished).

[45] I. R. Mukhamedshin, H. Alloul, G. Collin, and N. Blanchard, cond-mat/0402074 (unpublished).